Chinese Physics B

Observation of layer-dependent uniaxial charge density wave in a noble metal alloy superconductor β-$IrSn_4$

To cite this article before publication: Xiao Liu *et al* 2026 *Chinese Phys. B* in press https://doi.org/10.1088/1674-1056/ae69c6

Observation of layer-dependent uniaxial charge density wave in a noble metal alloy superconductor β-$IrSn_4$

Xiao Liu (刘 潇)[1,2#], Geng Li (李 更)[1,2,3#,*], Shiwei Diao (刁世伟)[4#], Haisen Liu (刘海森)[1,2], Zhen Zhao (赵 振)[1,2], Haitao Yang (杨海涛)[1,2,3], Lizhi Zhang (张礼智)[4*], Xiao Lin (林 晓)[1*], Hong-Jun Gao (高鸿钧)[1,2,3]

[1] *School of Physical Sciences, University of Chinese Academy of Sciences, Beijing 101408, China*

[2] *Beijing National Center for Condensed Matter Physics and Institute of Physics, Chinese Academy of Sciences, Beijing 100190, China*

[3] *Hefei National Laboratory, Hefei 230088, China*

[4] *Laboratory of Theoretical and Computational Nanoscience, National Center for Nanoscience and Technology, Beijing 100190 China*

The AB_4-type intermetallic compounds host a wide range of emergent quantum phenomena, providing a fertile platform for exploring the interplay between crystal structure and electronic orders. Among them, β-$IrSn_4$ has recently attracted attention as a noble-metal-based layered superconductor with weak interlayer coupling and type-I superconductivity. However, its electronic states and possible symmetry-breaking orders remain largely unexplored in atomic scale. Here, we report the observation of a layer-dependent uniaxial charge density wave (CDW) in β-$IrSn_4$ using ultra-low-temperature scanning tunneling microscopy. The charge order appears as stripe-like modulations that break the in-plane C_4 symmetry, and its orientation rotates by 90° between adjacent layers. Spectroscopy measurements reveal a homogeneous superconducting gap coexisting with the layer-dependent CDW, with no detectable modulation from the charge order. First-principles calculations suggest that interlayer coupling induces the observed anisotropic electronic structure. These results reveal a layer-dependent symmetry-breaking electronic state in β-$IrSn_4$ and highlight the role of interlayer interactions in shaping its electronic properties.

Keywords: charge density wave; layer-dependent; superconductivity; interlayer coupling

PACS: 71.45.Lr, 74.55.+v, 74.70.–b, 63.22.Np

[#]These authors contributed equally to this work.

[*]Correspondence to: xlin@ucas.ac.cn, zhanglz@nanoctr.cn, gengli.iop@iphy.ac.cn

Intermetallic compounds with the AB_4 stoichiometry constitute an important class of quantum materials, exhibiting diverse phenomena such as superconductivity [1-8] and nontrivial electronic topology. [1-4,7-15] Their rich structural motifs, often featuring complex coordination environments and layered stacking sequences, provide a natural platform for studying how lattice symmetry, dimensionality, and electronic interactions intertwine. In particular, the sensitivity of these systems to subtle structural variations makes them ideal candidates for uncovering emergent symmetry-breaking states and their coupling to collective electronic phases.

Among these materials, β-$IrSn_4$ stands out as a recently revisited system with intriguing physical properties. [6-8,10,16] It crystallizes in a layered structure composed of $IrSn_8$ square antiprisms, giving rise to quasi-two-dimensional electronic characteristics with finite interlayer coupling. Transport and thermodynamic measurements have identified β-$IrSn_4$ as a type-I superconductor with an exceptionally low critical field, [6-8] suggesting a conventional BCS pairing mechanism. Meanwhile, its noble-metal-based composition and relatively weak electronic correlations distinguish it from many strongly correlated charge density wave (CDW) systems, [17-25] raising the fundamental question of whether and how symmetry-breaking electronic orders can emerge in such a setting. Despite these intriguing properties, direct experimental access to its atomic-scale electronic structure has remained scarce.

Here, we report an atomic-scale investigation of β-$IrSn_4$ using scanning tunneling microscopy and spectroscopy at dilution refrigerator temperatures. We uncover a uniaxial charge density wave that spontaneously breaks the in-plane C_4 symmetry into C_2, forming stripe-like electronic modulations along one crystallographic axis. More strikingly, by systematically probing multiple terraces corresponding to different layers in the stacking sequence, we reveal that the CDW orientation alternates by 90° between adjacent layers, giving rise to a layer-dependent uniaxial CDW. This behavior is strictly locked to the crystallographic stacking and cannot be attributed to surface effects, indicating an intrinsic bulk electronic order governed by interlayer interactions. Concurrent spectroscopic measurements demonstrate a homogeneous superconducting gap that is insensitive to the CDW, defects, and step edges, suggesting weak or negligible coupling between superconductivity and charge order. Supported by first-principles calculations, our results establish a direct link between interlayer coupling and anisotropic electronic structure, providing new insight into how three-dimensional stacking can stabilize unconventional symmetry-breaking states even in weakly correlated intermetallic systems.

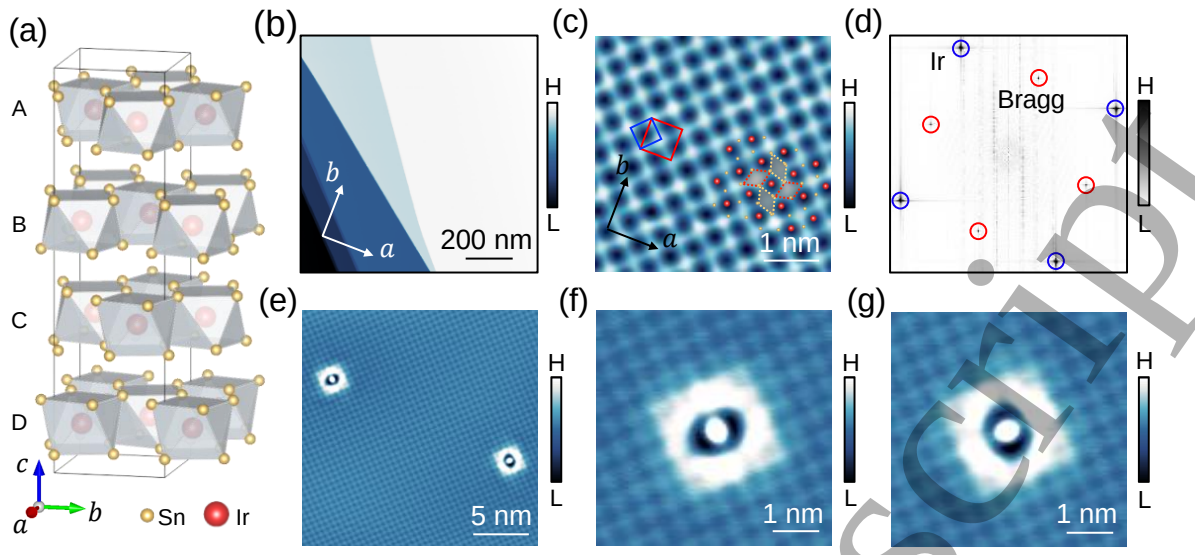

Fig. 1. Atomic model, surface topography and determination of as-cleaved Sn termination of β-$IrSn_4$. (a), Schematic illustration of the atomic structure of β-$IrSn_4$ with Ir and Sn atoms respectively denoted by red and yellow spheres. Each Ir atom is coordinated by a square antiprism (grey) formed by eight Sn atoms, with all $IrSn_8$ antiprisms interconnected through edge-sharing. The crystal structure shows an A-B-C-D stacking sequence along the *c*-axis. (b), STM topography of micron-scale atomically flat cleaved surface (V_s = -90 mV, I_t = 50 pA). (c), Atomically resolved STM images (V_s = -600 mV, I_t = 1 nA) showing a square lattice, with the schematic of an Ir atom layer and the subsequent Sn atom layer overlaid above. (d), FT of STM image of a typical area. Peaks corresponding to Bragg points (red circles) and Ir lattice (blue circles) are clearly visible, whose corresponding periodic units are represented by red and blue squares in panel (c). (e), STM image of two adatoms and its surrounding electronic states exhibiting perpendicular orientation (V_s = 1 V, I_t = 1 nA), whose equivalent positions are denoted by grey rhombi respectively bordered by red and yellow dashed lines in panel (c) which clarify two types of mutually perpendicular surface electronic environments. (f, g), The zoom-in view of the two adatoms and its surrounding electronic states in panel (e).

High-quality β-$IrSn_4$ single crystals were synthesized via a self-flux growth method. Energy dispersive X-ray spectroscopy and single crystal X-ray diffraction (Fig. S1) were done to confirm that the sample was in correct element ratio and in β phase. β-$IrSn_4$ crystallizes in the space group $I4_1/acd$ (#142), featuring a layered structure (Fig. 1(a)). Each Ir atom is coordinated by eight Sn atoms forming a $IrSn_8$ square antiprism. These edge-sharing antiprisms stack in A-B-C-D sequence along the *c*-axis to form the bulk crystal.

Scanning tunneling microscopy/spectroscopy (STM/S) measurements were carried out in a customized STM system under an ultrahigh vacuum of 1×10^{-10}mbar. The temperature at the STM sample holder was cooled down to 31 mK through ^{3}He-^{4}He dilution refrigeration. Tungsten tips, prepared by chemical etching, were annealed in ultrahigh vacuum to remove

surface oxides and adsorbed contaminants, and subsequently calibrated on a clean Au(111) surface prior to use. The sample was mechanically cleaved at liquid nitrogen temperature in an ultrahigh vacuum environment and immediately transferred to the STM sample holder. Differential conductance was acquired using a standard lock-in technique at a frequency of 932 Hz with an excitation voltage of one percent of the sample bias for stabilizing the tunneling junction.

We begin by characterizing the surface atomic structure and termination of cleaved β-$IrSn_4$. Large-scale STM topography reveals micron-scale atomically flat terraces on the cleaved surface (Fig. 1(b)). Atomic-resolution STM imaging (Fig. 1(c)) and its Fourier transform (FT) (Fig. 1(d)) confirm a square surface lattice. The most prominent periodicity observed in the real-space image and the most pronounced peaks in the FT correspond to a lattice with the period of ~ 0.45 nm, consistent with the known periodicity of the Ir atomic layer according to previous studies. [6,7,16] However, cleavage is expected to occur between the Sn layers of adjacent sandwich layers due to their larger interlayer spacing and weaker bonding. The atomic-resolution STM patterns observed across all terraces show the same feature and the step heights between terraces are integer multiples of $c/4$, indicating that the termination of cleavage is Sn layer.

To further confirm the Sn terminated surface, we found a type of adatoms with surrounding C_2 symmetry electronic environments, which might be Sn or Ir atoms induced by cleavage process. We also noticed that there is a sort of sites marked by the centers of the grey rhombi formed by four Sn atoms in Fig. 1(c) lying on two-fold rotation symmetry axes. Adjacent rhombi exhibit mutually perpendicular orientations, resulting in 90°-rotated electronic environments between neighboring rhombic center, leading to a rule: traversing an *even* number of steps along adjacent rhombic centers leads to identical electronic environments; traversing an *odd* number of steps yields perpendicular electronic environments. Intriguingly, two adatoms separated by 47 rhombic steps (Fig. 1(e)) display mutually perpendicular electronic states, while those two separated by 8 steps (Fig. S2(a)) show parallel orientations. The consistent observation of the orientations of these adatoms at their expected positions unequivocally confirms that the cleaved surface is Sn-terminated, and the atomic correspondence between the STM topography and the surface atomic structure is thus established, as depicted in Fig. 1(c). Furthermore, defects with C_4 symmetry are found at the dark points of the STM topography (Fig. S2(b)) which cannot be pushed away by the tip like the adatoms in Fig. 1. We attribute these defects to single Ir atom vacancies in subsurface layers because Ir atomic sites uniquely exhibit local

C_4 symmetry; the spatial coincidence of the black points in STM topography with Ir lattice sites gives further evidence of the aforementioned atomic correspondence. Unambiguously establishing this atomic registry through defect analysis is a crucial prerequisite, as it provides the exact structural input required for the subsequent theoretical modelling of the symmetry-breaking CDW state which will be discussed later.

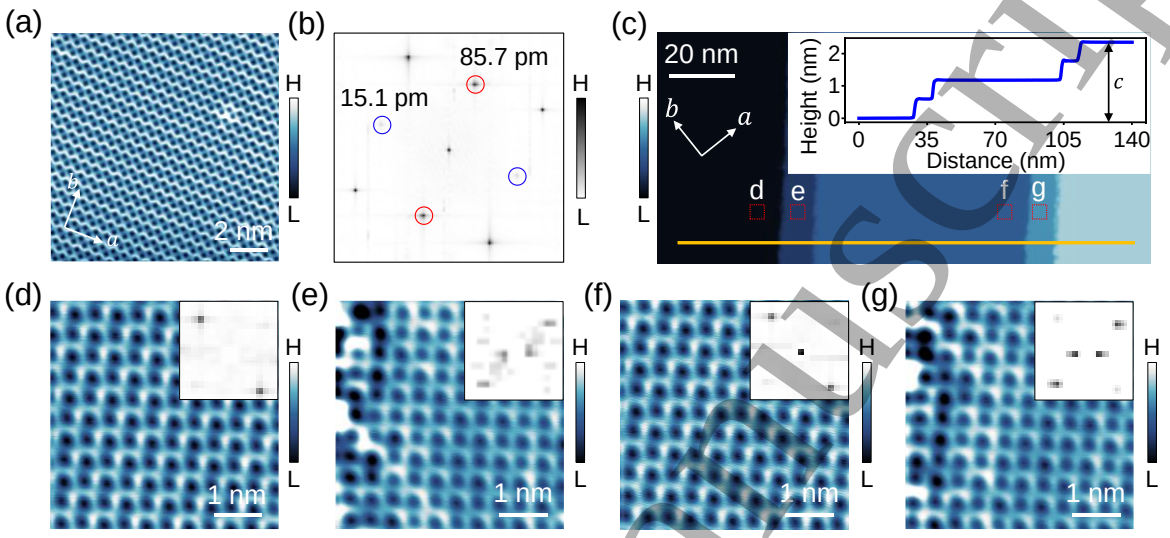

Fig. 2. Layer-dependent uniaxial charge density waves with perpendicular orientation. (a), Atomically resolved STM image showing uniaxial CDW stripes (V_s = 200 mV, I_t = 1 nA). (b), FT of the STM image in (a), exhibiting strongly anisotropic Bragg peaks with pronounced intensity contrast between orthogonal directions. (c), STM topography showing five consequent sandwich-layer terraces (V_s = 1 V, I_t = 50 pA). Inset: Height line profile at the yellow line, clarifying that the five terraces have height difference of a quarter of a unit cell consequently. (d-g), Zoom-in STM images at the corresponding red dashed square in panel (c) (V_s = 200 mV, I_t = 7 nA), showing alternating uniaxial CDW stripes with perpendicular orientation. Inset: FT image of each STM topography.

Further STM studies on the as-cleaved Sn terminated surface of β-$IrSn_4$ reveal a striking symmetry-broken electronic state. Atomically resolved topography, acquired under smaller tip-sample distance (~ 200 mV), exhibits pronounced commensurate $1a_0$ uniaxial CDWs manifesting as stripe-like patterns (Fig. 2(a)). These stripes consistently aligning along one of the two equivalent directions, crystallographic a or b axis, selectively enhances or suppresses the electronic states along specific Sn atom chains, which reduces the C_4 rotational symmetry to C_2 and breaks the mirror symmetry within the single sandwich layer. The anisotropic nature of this charge order is demonstrated by the FT of the STM image as well (Fig. 2(b)). The FT spectrum exhibits strongly anisotropic Bragg peaks, with significantly higher intensity along

the direction parallel to the observed stripes compared to the orthogonal direction.

To investigate the evolution of this CDW state across different layers, we systematically probed a region containing five consecutive atomic terraces separated by steps (Fig. 2(c)). STM topographic imaging at each terrace level confirmed the atomically flat nature of each layer. The height line profile across these terraces (inset, Fig. 2(c)) revealed that the step height between consecutive terraces is consistently equal to a quarter of the unit cell parameter of *c*-axis ($c/4 \sim 0.3$ nm), corresponding to the separation between Sn-terminated layers within the A-B-C-D stacking sequence. High-resolution STM imaging performed under identical tunneling conditions on each individual terrace (Fig. 2(d-g)) yielded a remarkable observation that the orientation of the uniaxial CDW stripes alternates between consecutive layers. Stripes on terraces separated by an odd multiple of the $c/4$ step height (e.g., between layers A and B, or B and C, etc.) exhibit perpendicular orientations. In contrast, stripes on terraces separated by an even multiple of the $c/4$ step height (e.g., between layers A and C, or B and D) share the same orientation. The FT of each individual terrace image (insets, Fig. 2(d-g)) consistently reflects this layer-dependent anisotropy, confirming the CDW direction for each layer.

This observation of layer-dependent uniaxial CDW with perpendicular alignment between adjacent Sn-terminated layers is highly reproducible across different sample regions and step configurations (Fig. S3). The strict dependence of the CDW orientation alternation on the $c/4$ step height rule robustly excludes the possibility of this phenomenon arising from artifacts related to the STM tip or from surface reconstructions confined to the topmost layer. Instead, it provides compelling evidence for an intrinsic, layer-dependent electronic ordering that breaks symmetry differently in consequent layers of the β-$IrSn_4$ crystal.

The electronic properties of β-$IrSn_4$ at low temperatures were probed using scanning tunneling spectroscopy (STS) at dilution refrigerator temperature (~ 31 mK). Spectroscopy measurements (Fig. 3(b)) reveal a clear superconducting (SC) gap signature in the differential conductance (dI/dV) spectrum. The spectrum exhibits a V-shaped gap structure centered at the Fermi level, with coherence peaks located at approximately ± 0.5 mV. A numerical fit based on the Dynes model [26] (solid line in Fig. 3(b)) shows consistency with the experimental data. The yielded gap value Δ is 0.158meV, resulting in a $2\Delta/k_BT_c$ ratio of 3.49 with the T_c assumed as 1.05 K reported by earlier study. [7] This ratio closely matches the isotropic BCS weak-coupling limit where it is 3.53. This gap structure is consistently observed across the sample surface, existing simultaneously with the layer-dependent uniaxial CDW. A dI/dV linecut across the CDW stripe is performed (Fig. 3(c, d)). To quantitatively evaluate the spatial uniformity of the

superconductivity, we performed Dynes model fitting on each individual spectrum along the linecut to extract the local gap size Δ, which is overlaid in Fig. 3(c, d). The extracted Δ exhibits an extremely small standard deviation of 0.001 mV, representing an upper bound of spatial modulation of merely ~0.63% relative to the average gap size. Such extraordinary spatial homogeneity establishes the weak or negligible coupling nature between the layer-dependent uniaxial CDW and the superconductivity.

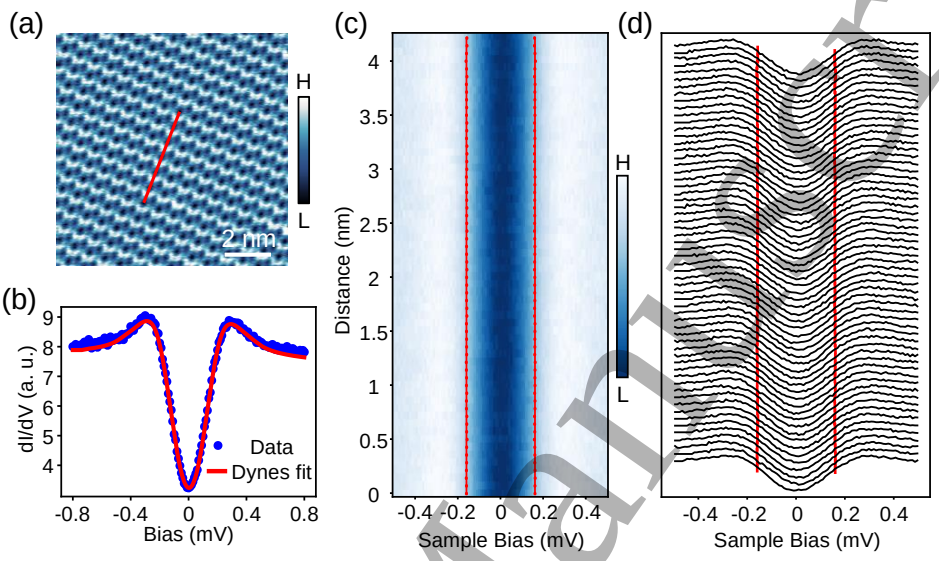

Fig. 3. Homogeneous superconductivity coexisting with uniaxial CDW stripes. (a), Atomically resolved STM image of a region with uniaxial CDW stripes (V_s = 200 mV, I_t = 5 nA). (b), Spatial average of 1024 dI/dV spectra and Dynes fit of the data, showing good consistency. (c), (d), Pseudo color map and waterfall plot of the dI/dV linecut along the red line in panel (a). The gap edge positions extracted from Dynes fitting of each spectrum are marked in panel (c) and (d), revealing high uniformity of the superconducting gap. For the data in panel (b), (c) and (d), tunneling junction was stabilized with parameters of V_s = 1 mV, I_t = 1 nA, lock-in parameters are V_{mod} = 10 μV and f = 932 Hz.

During the experiment, we find that the SC phase in β-$IrSn_4$ demonstrates exceptional sensitivity to magnetic fields, necessitating meticulous demagnetization of the instrumentation and sample to resolve the characteristic spectroscopic signatures. In magnetic field dependent experiments, the SC gap can only stay robustly at applied fields up to 6 mT. STS experiment across large area further reveals the absence of vortices and the homogeneity of the SC. Notably, while ramping up and down the magnetic field or varying the scanning box, the SC gap exhibits a stochastic emergence and disappearance for fields below 6 mT, but remains remarkably consistent in both shape and magnitude whenever it is resolved (Fig. S4).

Assuming the system is a type-II SC, the theoretical density of quantum flux vortices n at an applied magnetic field of B = 6 mT is 2.90 μm^{-2}. Given our typical large-scale scanning field of view (FOV) of 1.5 μm × 1.5 μm (yielding a total area of 2.25 μm^2), we would expect observe approximately 6 to 7 vortices within a single FOV. Empirically, for a type-II SC approaching its upper critical field, the vortices become densely packed. Under such conditions, a significant portion of the scanning area would be occupied by vortex cores and their surrounding halos within the FOV, leading to heavily suppressed SC gaps or zero bias peaks due to the vortex bound states during the STS measurements, which is inconsistent with our observation.

Instead, the behavior of the SC gaps under magnetic fields strongly suggests that the sample resides in the intermediate state of a type-I SC. Type-I SCs possess a positive surface energy between the normal and SC phases. Under a magnetic field below H_c, the system thermodynamically minimizes the interfacial area, driving a macroscopic or mesoscopic phase separation into coexisting normal puddles and SC domains in the presence of a finite demagnetization factor for bulk material. When the applied magnetic field is varied in proximity to H_c, the sample repeatedly transitions through this intermediate state. Notably, our STM scanning FOV is substantially smaller than the characteristic spatial extent of these macroscopic phase domains. Due to the fluctuation of our magnetic field controller in mT-level, the spatial redistribution of the normal and SC regions after each field variation is intrinsically random, giving rise to the stochastic emergence and disappearance of the SC gap captured by the localized STS measurements. These results provide microscopic experimental evidence for the classification of β-$IrSn_4$ as a rare compound type-I superconductor with an ultralow critical field (~ 6.8 mT). [6-8]

We also testified that the SC gap remains unmodulated by structural and electronic heterogeneities such as the underlying atomic lattice, stripes of the layer-dependent uniaxial CDW, multiple types of defects, and terrace step edges (Fig. S5-S7). Characterized by a Ginzburg-Landau parameter $\kappa = \lambda/\xi < 1/\sqrt{2}$, type-I SCs have a substantially large coherence length ξ, which far exceeds the characteristic length scales of the CDW and other atomic-scale structural modulations ($\xi \gg \lambda_{CDW}$). Thus, the highly extended order parameter spatially averages out these localized charge density perturbations. This offers a plausible explanation for the observed homogeneity of the SC state.

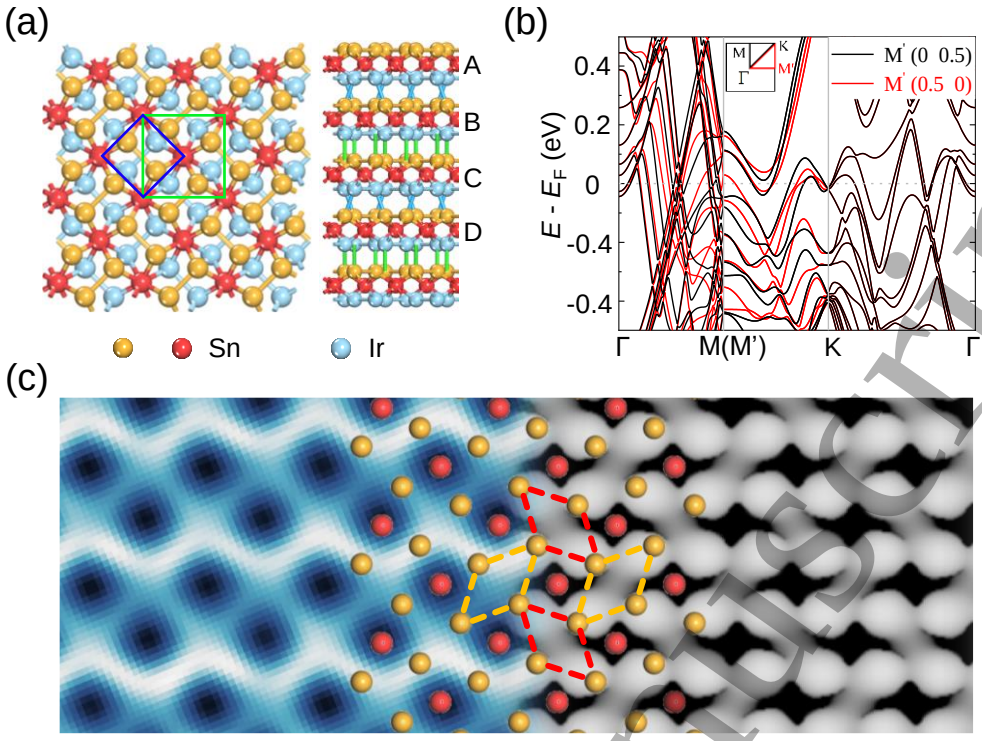

Fig. 4. Calculated configurations and electronic properties for the slab model. (a), Top and side view of the slab model. (b), Total band structures for the slab model with six $IrSn_4$ layers. (c), Atomically resolved experimental and simulated STM image at ~ 200 mV.

In order to understand the origin of the unconventional CDW pattern, we performed first-principles calculations by density functional theory (DFT). DFT calculations were performed in the Vienna *Ab initio* Simulation Package (VASP) [27,28] adopting the projector-augmented wave (PAW) method and the Perdew-Burke-Ernzerhof (PBE) [29] functional. The grimme-D3 method [30] was used to describe the van der Waals interaction between β-$IrSn_4$ layers [31]. A slab model containing six $IrSn_4$ layers was constructed to investigate the influence of interlayer interactions on surface electronic states. The vacuum layers for the slab models are larger than 15 Å. The atoms were fully relaxed until the force on each atom was less than 0.01 $eV \cdot Å^{-1}$ in all β-$IrSn_4$ systems. In Fig. 4(a), we provide the top and side views of this configuration. When only the top layer of the material is considered, the structure exhibits C_4 symmetry, meaning the material is identical along the *a* and *b* directions, which is also supported by the calculated band structure for the monolayer β-$IrSn_4$ (shown in Fig. S8). However, for the multilayer slab model, as shown in the side view of Fig. 4(a), the differences in interlayer interactions can be clearly observed. For instance, the orientation of adjacent Sn atoms between layers A and B (blue line) is at a 90° angle to that between layers B and C (green line). In this case, the entire

system transforms to C_2 symmetry, which implies that the electronic structure may differ along the *a* and *b* directions. In Fig. 4(b), we provide the total band structures for the slab model containing six $IrSn_4$ layers. By comparing the bands along different directions (Γ-M vs Γ-M'), we can differentiate the bands shift due to the interlayer interactions from the second layer. In Fig. 4(c), we also present the simulated STM images, which clearly show good agreement with the experimental results and exhibit a transition from four-fold to two-fold symmetry, confirming that the emergence of CDW is induced by interlayer interactions.

In Fig. S9, we also performed density functional perturbation theory (DFPT) calculations to explore the potential BCS superconductivity of β-$IrSn_4$ via the QUANTUM ESPRESSO package. [32] The relativistic norm-conserving ONCV pseudopotentials [33] combined with the PBE exchange-correlation functional [29] were adopted. A plane-wave cutoff energy of 50 Ry, a *k*-mesh of 12 × 12 × 12 and a Marzari-Vanderbilt smearing of 0.01 Ry were employed in calculating the electronic states. The dynamical matrices and EPC matrices were computed by density functional perturbation theory using a *q*-mesh of 3 × 4 × 2. The Eliashberg spectral function $a^2F(\omega)$ was calculated by:

$$a^2F(\omega)=\frac{1}{2\pi N(E_F)}\sum_{qv}\frac{\gamma_{qv}}{\omega_{qv}}\delta(\omega-\omega_{qv}), \qquad (1)$$

where γ_{qv} is the phonon linewidth, ω_{qv} is the phonon eigen frequency, and $N(E_F)$ is the electronic DOS at Fermi level. The projected phonon DOS and Eliashberg spectral function show that the transition metal Ir atoms make dominant contributions to the electron-phonon coupling (EPC) of β-$IrSn_4$. The EPC constant λ was calculated by:

$$\lambda=2\int_0^{\infty}\frac{\alpha^2F(\omega)}{\omega}d\omega. \qquad (2)$$

From this, we obtained a relatively strong EPC strength $\lambda = 0.365$. The superconducting critical temperature was estimated by using McMillan-Allen-Dynes formula: [34]

$$T_c=\frac{\omega_{log}}{1.2}\exp\left(-\frac{1.04(1+\lambda)}{\lambda-\mu^*(1+0.62\lambda)}\right), \qquad (3)$$

where ω_{log} = 249.65 K is the logarithmic average of the phonon frequency, and μ^* is the effective Coulomb repulsion constant. Here, we obtained $\mu^* = 0.26N(0)/(1+N(0)) = 0.127$, [35] where $N(0) = 0.961$ eV^{-1} is the DOS per transition metal atom. We estimated a $T_c \sim 0.9$ K for bulk β-$IrSn_4$, which is close to the experimental result of 1.05 K. [7] This suggests that β-$IrSn_4$ is very likely to be a BCS superconductor. Due to the long distance between two nearest Ir layers (~5.9Å), the influence of interlayer vibration on the superconductivity of β-$IrSn_4$ is

relatively weak, which is confirmed by the experimental results, where the uniform SC gaps are found along the *a* and *b* directions.

In summary, we have performed an atomic-scale study of the noble-metal intermetallic superconductor β-$IrSn_4$ using ultra-low-temperature scanning tunneling microscopy and spectroscopy. We identify a uniaxial charge density wave that breaks the in-plane C_4 symmetry and, more importantly, exhibits a layer-by-layer alternation of orientation following the intrinsic stacking sequence, forming a layer-dependent uniaxial CDW. This alternating behavior is robust and closely tied to the crystallographic structure, indicating an intrinsic electronic order governed by interlayer coupling. Meanwhile, a homogeneous superconducting gap is observed to coexist with the CDW without detectable modulation, suggesting a weak coupling between the two orders. First-principles calculations reveal that interlayer interactions can induce the observed anisotropic electronic structure.

References

[1] Shen D, Kuo C N, Yang T W, Chen I N, Lue C S and Wang L M 2020 *Commun. Mater.* **1** 56.

[2] Zhu W, Song R, Huang J, et al. 2023 *Nat. Commun.* **14** 7012.

[3] Ye Y, Song R, Xiao H, Xian G, Guo H, Yang H, Chen H and Gao H-J 2024 *Nano Lett.* **24** 13455.

[4] Xu C Q, Li B, Zhang L, Pollanen J, Yi X L, Xing X Z, Liu Y, Wang J H, Zhu Z, Shi Z X, Xu X and Ke X 2021 *Phys. Rev. B* **104** 125127.

[5] García Talavera P, Moreno J A, Herrera E, Buzdin A I, Bud'ko S L, Canfield P C, Guillamón I and Suderow H 2025 *J. Supercond. Nov. Magn.* **38** 158.

[6] Tran V H, Bukowski Z, Wiśniewski P, Tran L M and Zaleski A J 2013 *J. Phys.: Condens. Matter* **25** 155701.

[7] Ahmad N, Shimada S, Hasegawa T, Suzuki H, Afzal M A, Nakamura N, Higashinaka R, Matsuda T D and Aoki Y 2024 *J. Phys. Soc. Jpn.* **93** 044706.

[8] Speer S, Pershin Y V, Blawat J, Singleton J and Jin R 2026 *J. Phys.: Condens. Matter* **38** 055702.

[9] Wu H, Hallas A M, Cai X, Huang J, Oh J S, Loganathan V, Weiland A, McCandless G T, Chan J Y, Mo S-K, Lu D, Hashimoto M, Denlinger J, Birgeneau R J, Nevidomskyy A H, Li G, Morosan E and Yi M 2022 *npj Quantum Mater.* **7** 31.

[10] Mai T L and Tran V H 2022 *RSC Adv.* **12** 17882.

[11] Mun E, Ko H, Miller G J, Samolyuk G D, Bud'ko S L and Canfield P C 2012 *Phys. Rev. B* **85** 035135.

[12] Wang Y J, Liang D D, Ge M, Yang J, Gong J X, Luo L, Pi L, Zhu W K, Zhang C J and Zhang Y H 2018 *J. Phys.: Condens. Matter* **30** 155701.

[13] Li G, Fu C, Shi W, et al. 2019 *Angew. Chem., Int. Ed.* **58** 13107.

[14] Satheasuweatha M N, Mariappan S, Maran T, Kuo C N, Lue C S, Sonachalam A and Joseph B 2025 *Phys. Status Solidi RRL* **19** 2500126.

[15] Sahu S, Chen D, Heinsdorf N, Warner A N, Altthaler M, Singh A K, Bonn D A, Burke S A and Hallas A M 2025 *Commun. Mater.* **6** 244.

[16] Nordmark E-L, Wallner O and Häussermann U 2002 *J. Solid State Chem.* **168** 34.

[17] Tranquada J M, Sternlieb B J, Axe J D, Nakamura Y and Uchida S 1995 *Nature* **375** 561.

[18] Sipos B, Kusmartseva A F, Akrap A, Berger H, Forró L and Tutiš E 2008 *Nat. Mater.* **7** 960.

[19] Chang J, Blackburn E, Holmes A T, Christensen N B, Larsen J, Mesot J, Liang R, Bonn D A, Hardy W N, Watenphul A, Zimmermann M V, Forgan E M and Hayden S M 2012 *Nat. Phys.* **8** 871.

[20] Ghiringhelli G, Le Tacon M, Minola M, Blanco-Canosa S, Mazzoli C, Brookes N B, De Luca G M, Frano A, Hawthorn D G, He F, Loew T, Sala M M, Peets D C, Salluzzo M, Schierle E, Sutarto R, Sawatzky G A, Weschke E, Keimer B and Braicovich L 2012 *Science* **337** 821.

[21] Comin R, Frano A, Yee M M, Yoshida Y, Eisaki H, Schierle E, Weschke E, Sutarto R, He F, Soumyanarayanan A, He Y, Le Tacon M, Elfimov I S, Hoffman J E, Sawatzky G A, Keimer B and Damascelli A 2014 *Science* **343** 390.

[22] Chen H, Yang H, Hu B, et al. 2021 *Nature* **599** 222.

[23] Teng X, Chen L, Ye F, et al. 2022 *Nature* **609** 490.

[24] Yin J-X, Jiang Y-X, Teng X, et al. 2022 *Phys. Rev. Lett.* **129** 166401.

[25] Shi X, Liu X, Li G, Zhao Z, Yang H, Lin X and Gao H-J 2025 *Chin. Phys. B* **34** 077101.

[26] Dynes R C, Narayanamurti V and Garno J P 1978 *Phys. Rev. Lett.* **41** 1509.

[27] Kresse G and Hafner J 1993 *Phys. Rev. B* **47** 558.

[28] Kresse G and Furthmüller J 1996 *Comput. Mater. Sci.* **6** 15.

[29] Perdew J P, Burke K and Ernzerhof M 1996 *Phys. Rev. Lett.* **77** 3865.

[30] Grimme S, Antony J, Ehrlich S and Krieg H 2010 *J. Chem. Phys.* **132** 154104.

[31] Dion M, Rydberg H, Schröder E, Langreth D C and Lundqvist B I 2004 *Phys. Rev. Lett.* **92** 246401.

[32] Giannozzi P, Baroni S, Bonini N, et al. 2009 *J. Phys.: Condens. Matter* **21** 395502.

[33] Schlipf M and Gygi F 2015 *Comput. Phys. Commun.* **196** 36.

[34] Allen P B and Dynes R C 1975 *Phys. Rev. B* **12** 905.

[35] Zheng F, Li X-B, Tan P, Lin Y, Xiong L, Chen X and Feng J 2020 *Phys. Rev. B* **101** 100505.

Acknowledgments

Project supported by the National Key Research and Development Projects of China (2024YFA1207700, 2024YFA1207800, 2022YFA1204100), National Natural Science Foundation of China (62488201, 61925111, U23A6015), the CAS Project for Young Scientists in Basic Research (YSBR-003), the Youth Innovation Promotion Association (2023005), and the Quantum Science and Technology-National Science and Technology Major Project (2021ZD0302700).